J Solid State Electrochem (2012) 16:2957–2966
DOI 10.1007/s10008-012-1701-z

ORIGINAL PAPER

Gold nanoparticles on a thiol-functionalized silica network for ascorbic acid electrochemical detection in presence of dopamine and uric acid

Andréia de Morais · Gustavo Silveira · Paulo César Mendes Villis · Camila Marchetti Maroneze · Yoshitaka Gushikem · Fábio Luiz Pissetti · Alzira Maria Serpa Lucho

Received: 3 March 2011 / Revised: 21 February 2012 / Accepted: 22 February 2012 / Published online: 29 March 2012

Abstract A simple preparation methodology able to stabilize gold nanoparticles and to obtain an electrode which detects ascorbic acid, uric acid, and dopamine by different techniques is presented. A 3-mercaptopropyl-functionalized silica network was synthesized using the sol–gel method. Gold nanoparticles (nAu) were immobilized on the material at synthesis by adding a sol of these previously prepared particles to the reaction mixture. The electrochemical behavior of the SiO_2/MPTS/Au carbon paste electrode was studied using cyclic voltammetry in the presence of a hexacyanoferrate probe molecule. The presence of nAu in the functionalized silica network changes the electrochemical characteristics of the material, favoring the electron transfer process of this complex ion. The SiO_2/MPTS/Au electrode was proven to be an efficient tool in the simultaneous determination of ascorbic acid (H_2AA), dopamine (DA), and uric acid (UA) using square wave voltammetry techniques. With the nAu on the electrode, an increase in the peak current related to the redox process of the H_2AA, DA, and UA was observed. The separations of the anodic peak potentials between DA/H_2AA and UA/H_2AA were 310 and 442 mV, respectively. The results obtained show that the SiO_2/MPTS/Au electrode can be used in the simultaneous determination of H_2AA, DA, and UA.

Keywords Gold nanoparticles · Sol–gel · Thiol · Ascorbic acid · Simultaneous determination

A. de Morais · G. Silveira · P. C. M. Villis · F. L. Pissetti · A. M. S. Lucho (✉)
Instituto de Química, Universidade Federal de Alfenas,
700 Gabriel Monteiro da Silva Street,
37130-000 Alfenas, MG, Brazil
e-mail: lucho@unifal-mg.edu.br

C. M. Maroneze · Y. Gushikem
Laboratório de Química de Superfície, Instituto de Química,
Universidade Estadual de Campinas,
P.O. Box 6154, 13084-971 Campinas, SP, Brazil

Introduction

Metallic nanoparticles (MNPs) have attracted considerable attention recently because of several studies dealing with their synthesis, modification, properties, and applications. This interest is mainly due to the remarkable and unique properties presented by these particles that are not available in their bulk equivalent, e.g., high surface/volume ratios and quantum confinement effects. The use of these properties in technological applications has enabled exponential advancements in materials science and has led to the discovery of new ways of handling and manufacturing materials at the nano level [1–4].

The importance of gold nanoparticles (nAu) is highlighted by a wide range of applications in areas such as controlled drug delivery systems [5], electronic and optical devices [6], medical diagnosis [7], catalysis [1], sensors [8], and biosensors [9]. In particular, the physicochemical properties of nAu make them very attractive and suitable for the modification of conventional electrodes and the development of new electrode materials. The introduction of MNPs in electrochemical sensors and biosensors is a result of their large specific surface area, good biocompatibility, and

excellent catalytic properties, which significantly decrease the overpotential of many electrochemical reactions [9–11].

Although NPs provide a significantly higher number of electroactive centers in electroanalysis than the bulk metals, the NP free surface energy often leads to particle growth or aggregation and the loss of important properties achieved at the nano level. To avoid the inherent instability associated with particles of this size, the combination of synthesis procedures and effective MNP immobilization methods is extremely important. Porous solids with rigid frameworks, such as carbonaceous materials and inorganic oxides like silica, alumina, and titania, have been considered as alternatives to support and stabilize the MNPs [12, 13]. Most studies featuring supported metal nanoparticles have been related to heterogeneous catalysis because the rigid framework of porous solids usually offers high thermal and chemical stability and a large NP surface area, which are important properties for catalytic applications.

In the field of electroanalysis, sol–gel methodology has proven to be a useful tool in the preparation of silica-based functional materials [14–16], ranging from pure inorganic and mixed oxides [17, 18] to the more chemically complex hybrid organic–inorganic solids [19], which have been successfully applied in electroanalysis as working electrode materials.

Ascorbic acid (H_2AA), dopamine (DA), and uric acid (UA) are electroactive compounds of great biological and chemical interest that play important roles in human health. Sensing of these analytes is of great interest since H_2AA, DA, and UA coexist in the extracellular fluid of the central nervous system and serum. As they have similar oxidation potentials at most conventional electrodes, separate determination of these species is difficult due to their overlapped signals [20, 21]. Thus, the development of efficient electrodes with enhanced characteristics to distinguish these species in mixtures is a very important subject.

Striving to combine the remarkable properties of MNPs and the benefits offered by porous solids, the present work describes the synthesis, characterization, and application of a system consisting of nAu supported on the thiol groups (−SH) of an organofunctionalized silica network synthesized by sol–gel process.

Experimental

Reagents and solutions

All reagents used were of analytical grade and were used without any further purification. Phosphate buffer solutions (0.10 mol L^{-1}) were prepared using phosphoric acid and potassium hydroxide. The stock solutions of dopamine, ascorbic acid, and uric acid were prepared in the phosphate buffer solutions described above.

Preparation of gold nanoparticles

An aqueous chloroauric acid solution (95.0 mL) containing 5.0 mg of Au was brought to a boil and vigorously stirred in a round-bottom flask fitted with a reflux condenser. After it, 5.0 mL of aqueous 1 wt.% sodium citrate solution was added to the flask. This mixture was refluxed for 30 min. The solution changed color from pale yellow to deep red. The system was allowed to cool to room temperature with continuous stirring and was stored in a dark bottle until further use. This method yields quasi-spherical particles with an average diameter of about 10 nm [22, 23].

Synthesis of SiO_2/MPTS/Au

The thiol-functionalized silica network was prepared using the sol–gel process according to the following procedure. First, 10.0 mL of tetraethylorthosilicate was initially prehydrolyzed in ethanol solution (1:1 *v*/*v*) with 3.2 mL of distilled water; this reaction was catalyzed by HCl. The solution was stirred and heated at 353 K for 5 h. Next, 4.8 mL of (3-mercaptopropyl)-trimethoxysilane was added to this mixture, and then the mixture was stirred for 3 h at 353 K. At room temperature, 2.0 mL of the sol containing nAu was added to this solution. The temperature of the system was raised to 333 K until gel formation and then heated to 353 K to complete the solvent evaporation. The xerogel was washed with ethanol in a Soxhlet extractor and dried under vacuum. The obtained material was designated as SiO_2/MPTS/Au. Thiol-functionalized silica (SiO_2/MPTS) was also prepared by the same procedure in the absence of the AuNP sol.

Characterization

The FT IR spectrum of the material was obtained using a pressed KBr disk (1.0 wt.%) on a Bomem MB series FT IR with a 4 cm^{-1} resolution and 50 cumulative scans. Solid-state nuclear magnetic resonance spectroscopy for ^{13}C (CP/MAS NMR) was performed on a Bruker AC300/P spectrometer using pulse sequences with 4 ms contact time, an interval of 1 s between pulses, and an acquisition time of 41 ms. UV–vis absorption spectra were collected on a UV–vis NIR Cary-5 2300 spectrometer equipped with a diffuse reflectance accessory, and barium sulfate was used as a reference. Transmission electron microscopy (TEM) images were obtained on JEOL JEM-1220 microscope operating at 120 kV.

The electrochemical measurements were carried out using a PGSTAT 128 N Autolab® potentiostat–galvanostat. All experiments were carried out in a conventional three-electrode system with a platinum wire and a saturated calomel electrode as the counter and reference electrodes, respectively. The working

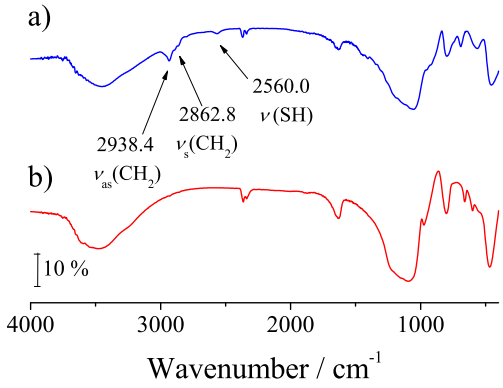

Fig. 1 Infrared spectra of (*a*) SiO_2/MPTS/Au and (*b*) silica gel

electrode was prepared by mixing SiO_2/MPTS/Au and graphite powder in a 3:2 (wt) proportion to obtain an adequate consistency and electrochemical behavior. The mixture was deposited into a cavity (1.0 mm in depth) in contact with a platinum disk (0.50 cm in diameter) fused at the end of a glass tube. The gold, platinum, and vitreous carbon electrodes have a geometric area of 0.15 cm^2. The following instrument parameters were used to record the square wave voltammograms: 10 mV square wave amplitude, 10 Hz frequency, and 19.5 mV step potential.

Results and discussion

Characterization of the SiO_2/MPTS/Au

The main characteristic absorption bands of SiO_2/MPTS/Au (Fig. 1a) are in the 3,020−2,800 cm^{-1} range and can be attributed to the C−H asymmetric and symmetric stretching vibrations of the $-CH_2$ groups. The spectrum also shows C−H deformation of $-CH_2$ groups at 1,440 cm^{-1} and a weak band at 2,560 cm^{-1} assigned to the S−H stretching vibration. The other absorption bands were the same for the absorption spectrum of silica gel (Fig. 1b) and can be assigned as follows: 1,200–1,100 cm^{-1} (ν_{AS} Si−O−Si), 920 cm^{-1} (ν_S Si−O of the silanol group), 795 cm^{-1} (ν_S Si−O of the siloxane group), 690 cm^{-1} (ν_S Si−O−Si), and 456 cm^{-1} (δ Si−O−Si). A broad absorption band between 3,750 and 3,000 cm^{-1} is assigned to both the O−H stretching mode of silanol groups and the remaining adsorbed water [24, 25].

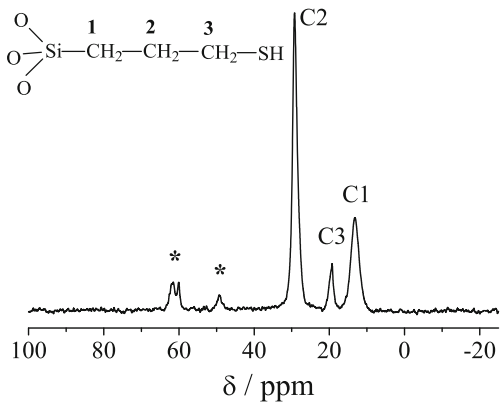

Fig. 2 ^{13}C CP-MAS NMR of SiO_2/MPTS/Au

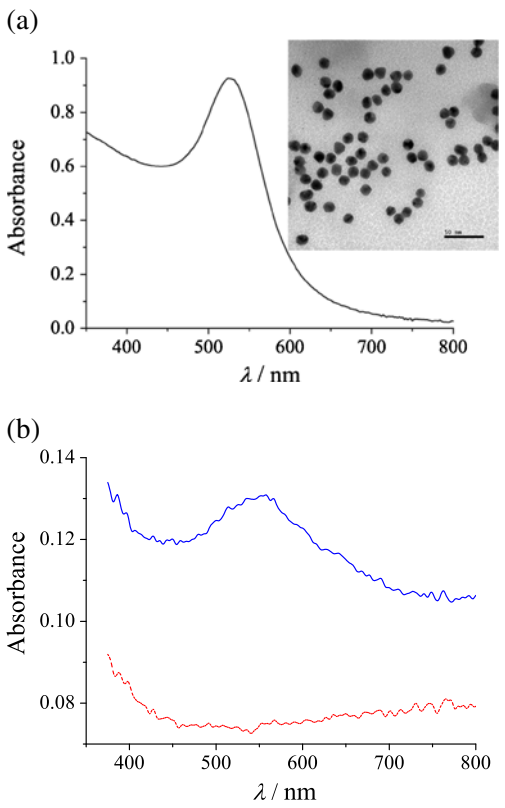

Fig. 3 **a** UV–vis spectra for gold nanoparticles sol. *Inset*, TEM of nAu sol. **b** Diffuse reflectance absorption spectra of SiO_2/MPTS (*dashed line*) and SiO_2/MPTS/Au (*solid line*)

The solid state ^{13}C CP-MAS NMR spectra for SiO_2/MPTS/Au show three signals with specific peak positions

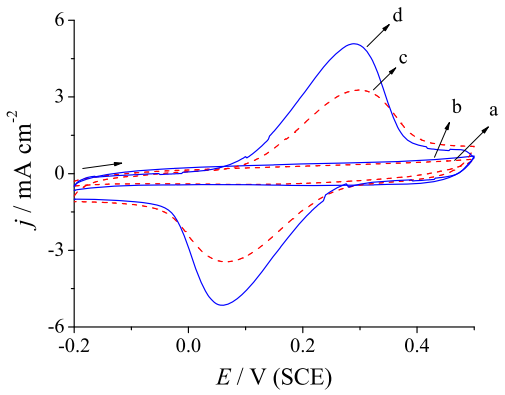

Fig. 4 Cyclic voltammograms (CVs) for SiO_2/MPTS (*a*, *c*) and SiO_2/MPTS/Au (*b*, *d*) electrodes in the absence (*a*, *b*) and presence (*c*, *d*) of 5.0 mmol L^{-1} $K_3Fe(CN)_6$ obtained with a 20 mV s^{-1} scan rate in 0.10 mol L^{-1} KCl solution

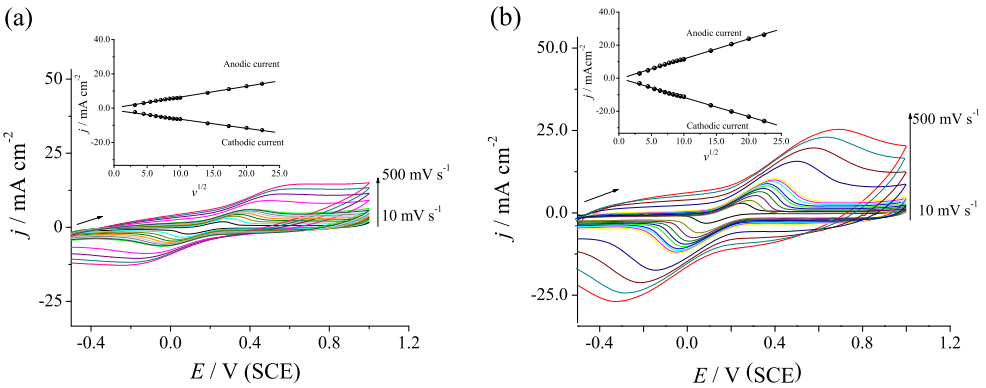

Fig. 5 Cyclic voltammograms for **a** SiO_2/MPTS and **b** SiO_2/MPTS/Au electrodes in 0.10 mol L^{-1} KCl containing 5.0 mmol L^{-1} $K_3Fe(CN)_6$ obtained with scan rates between 10 and 500 mV s^{-1}. The *insets* show the dependence of the peak current on the square root of the scan rate

at 13.2, 19.2, and 29.3 ppm, which can be assigned according to the carbon atoms numbered in the inset [26, 27]. The weak signals at 49.2 and 61.5 ppm are assigned to unhydrolyzed ethoxy and methoxy groups, respectively [28] (Fig. 2).

The optical properties of metal nanoparticles can be correlated with nanoparticle size, shape, and dielectric environment [3]. The UV–vis spectrum of nAu sol was obtained before incorporation of nAu in the SiO_2/MTPS material (Fig. 3a). This result displays a single surface plasmon resonance (SPR) band of Au nanoparticles, centered at 525 nm, which corresponds to a particle diameter smaller than 30 nm [29]. The inset in Fig. 3a presents the transmission electron microscopy of gold nanoparticles in colloidal solution. The image shows that nAu are quasi-spherical with a narrow size distribution. Diffuse reflectance spectroscopy measurements were carried out to detect the presence of nAu at prepared material. The UV–vis spectrum of SiO_2/MPTS (Fig. 3b) shows no absorption band. However, the SiO_2/MPTS/Au spectrum (Fig. 3b) displays a single SPR band centered at 540 nm. This result indicates that nAu were immobilized on the functionalized silica network. The verified shift, as compared to sol spectrum, can be attributed to a different medium permittivity at the solid state and the interaction between the nAu and sulfur in the functionalized silica network [29–31].

Electrochemical study of the SiO_2/MPTS/Au

The redox behavior of an electroactive species such as a $[Fe(CN)_6]^{3-/4-}$ couple is a valuable tool for evaluating the kinetic barrier of the electrode/solution interface [32].

The cyclic voltammetry response shows that no faradaic current was observed at curves a and b in Fig. 4 because there is no species in the solution that can be oxidized or reduced within this potential range. The electrochemical responses obtained for the SiO_2/MPTS and SiO_2/MPTS/Au electrodes were similar. In contrast, curves c and d in Fig. 4 show the oxidation peak of $[Fe(CN)_6]^{4-}$ ions at 0.29 V and the corresponding reduction peak at 0.06 V. The SiO_2/MPTS/Au electrode showed a 0.23 V peak potential separation ($\Delta E_p = E_{ANODIC\ PEAK} - E_{CATHODIC\ PEAK}$) and a 0.978 current ratio ($I_{ANODIC\ PEAK}/I_{CATHODIC\ PEAK}$). A significant current increase related to the $[Fe(CN)_6]^{3-/4-}$ redox processes was also observed when the nAu were bonded onto the functionalized silica network.

The peak current is directly proportional to the square root of the scan rate as shown in Fig. 5. This behavior indicates that the process is controlled by $[Fe(CN)_6]^{3-/4-}$ diffusion to the electrode/solution interface. Therefore, the slope of the two curves obtained from the SiO_2/MPTS/Au electrode (Fig. 5b) is larger than the slope of the curves from the SiO_2/MPTS electrode (Fig. 5a). This can be related to

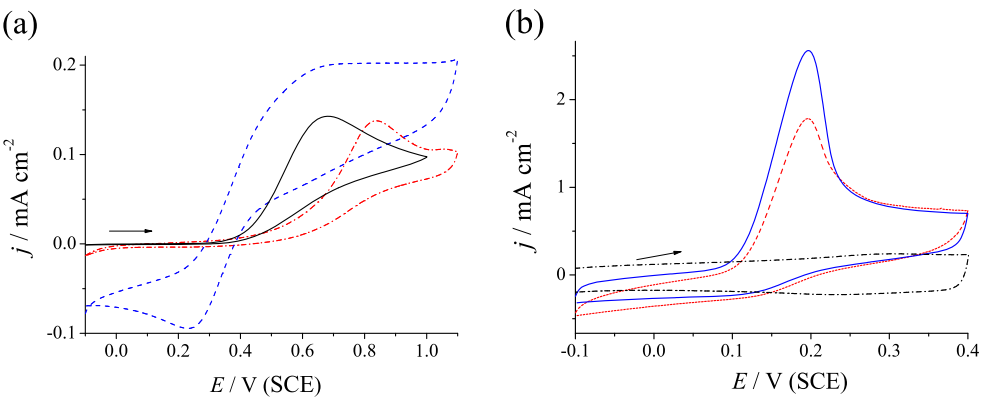

Fig. 6 **a** Cyclic voltammograms for platinum (*dashed line*), glassy carbon (*solid line*), gold electrodes (*dash-dotted line*), and **b** SiO_2/MPTS (*dashed line*) and SiO_2/MPTS/Au (*solid line*) electrodes in 0.10 mol L^{-1} phosphate buffer solution (pH 2.0) containing 2.0 mmol L^{-1} H_2AA. SiO_2/MPTS/Au (*dash-dotted line*) without H_2AA. All CV are obtained with a 10 mV s^{-1} scan rate

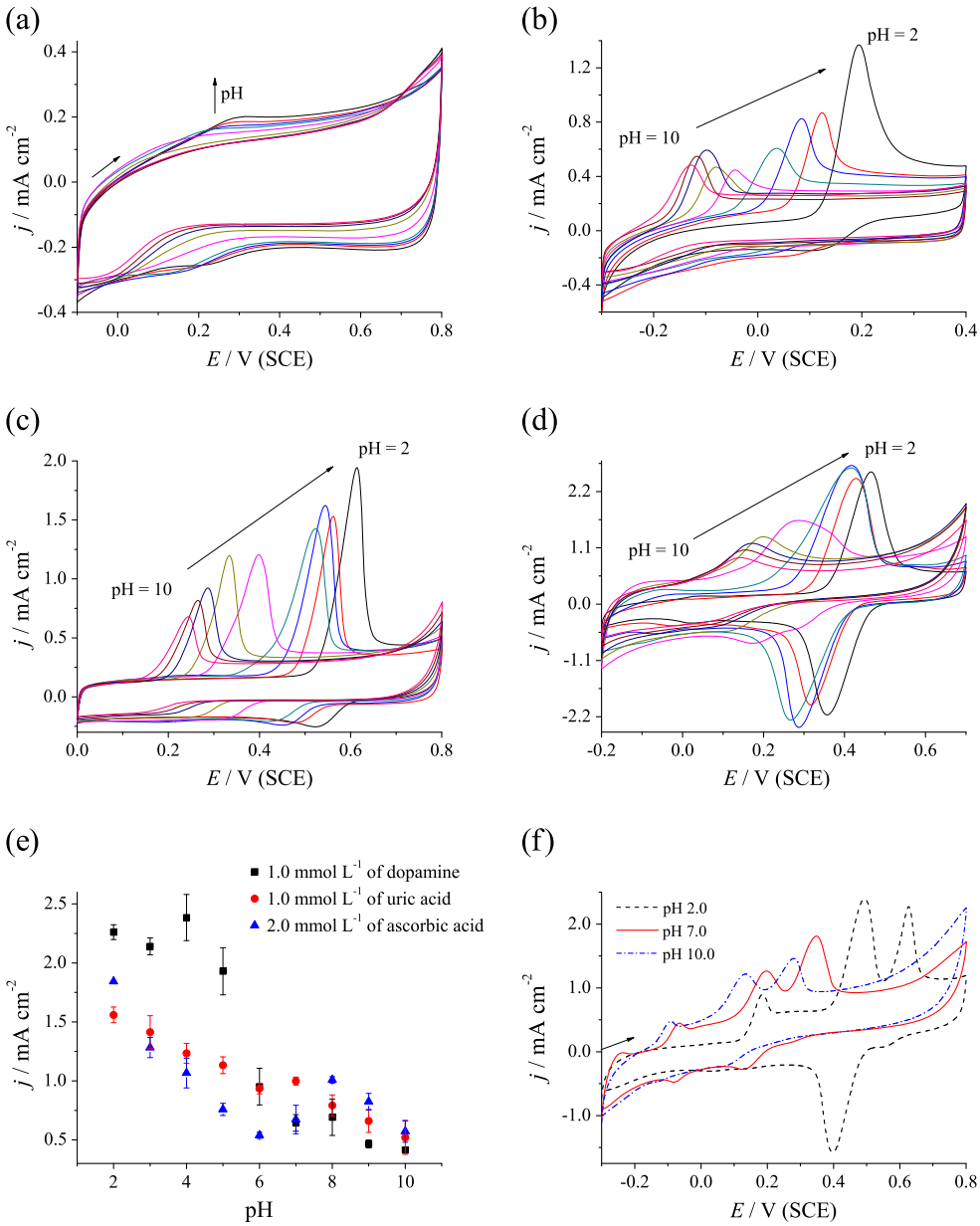

Fig. 7 **a** Cyclic voltammograms for SiO_2/MPTS/Au electrode from pH 2 to 10, **b** containing 2.0 mmol L^{-1} of H_2AA, **c** containing 1.0 mmol L^{-1} of DA, **d** containing 1.0 mmol L^{-1} of UA. **e** Oxidation peak current density for the three analytes in all studied pH. **f** Containing the three analytes simultaneously. All CVs are obtained with a 10 mV s^{-1} scan rate

the presence of nAu immobilized on a functionalized silica network that favors electron transfer at the electrode/solution interface. Also, one can observe that as the scan rate increased, the peak current related to the redox processes of $[Fe(CN)_6]^{3-/4-}$ also increased. Moreover, the peaks at high scan rates are not well defined for the SiO_2/MPTS electrode (Fig. 5a), unlike the peaks for the SiO_2/MPTS/Au electrode (Fig. 5b).

Electrocatalytic oxidation of ascorbic acid

Electrocatalytic oxidation of H_2AA was studied to evaluate the potential use of SiO_2/MPTS/Au material for electrochemical sensor.

Significant diminution of the oxidation potential occurs at the SiO_2/MPTS as compared to the values for conventional electrodes (Fig. 6a, b). The peak of current density in the anodic scan at approximately 0.190 V (Fig. 6b) can be assigned to the electro-oxidation of H_2AA. [33–35]. In addition, the current density at oxidation potential was approximately ten times higher for the SiO_2/MPTS electrode than for the bare platinum electrode, probably due to porosity of the material. Higher oxidation current density was observed for the electrode containing nAu, which can be attributed to an increase of the surface area due to the presence of the nanoparticles.

In most cases, the solution pH is an important factor in the electrochemical reaction. Cyclic voltammetry was performed

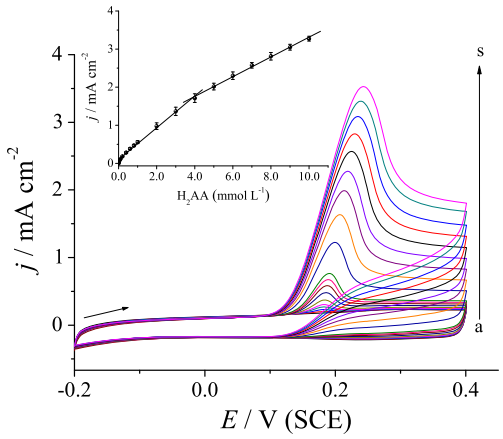

Fig. 8 Cyclic voltammograms for the SiO_2/MPTS/Au electrode in 0.10 mol L^{-1} phosphate buffer solution (pH 2.0) with different H_2AA concentrations: (*a*) 0, (*b*) 0.0060, (*c*) 0.020, (*d*) 0.050, (*e*) 0.10, (*f*) 0.20, (*g*) 0.40, (*h*) 0.60, (*i*) 0.80, (*j*) 1.0, (*l*) 2.0, (*k*) 3.0, (*m*) 4.0, (*n*) 5.0, (*o*) 6.0, (*p*) 7.0, (*q*) 8.0, (*r*) 9.0, and (*s*) 10.0 mmol L^{-1}. A scan rate of 10 mV s^{-1} was used. *Inset*, plot of the anodic peak current density (*j*) versus ascorbic acid concentration [H_2AA]

to study the solution pH effects on the electro-oxidation behavior of H_2AA, DA, and UA at the SiO_2/MPTS/Au electrode. The decrease of oxidation peak potential and current density with pH was observed (Fig. 7b–e). For the three analytes present simultaneously in solution, the highest current density for the oxidation process and the larger peak separation was observed at pH 2 (Fig. 7f). Considering these results, a 0.10 mol L^{-1} phosphate buffer solution with pH 2.0 was chosen as a supporting electrolyte for the experiments on electrochemical detection of H_2AA. The redox process for the species studied involves proton and electron transfer, which can explain the changes of the peak potential and current density with solution pH [36–38].

The oxidation current (Fig. 8) presented a linear behavior within the two H_2AA concentration ranges: 0.050 to 4.0 and 4.0 to 10.0 mmol L^{-1}. The inset in the figure depicts the analytical curve obtained by the SiO_2/MPTS/Au electrode in the two concentration ranges, with correlation coefficients of 0.9959 for n=13 and 0.9989 for n=7. The decrease in sensitivity in the second linear range is attributed to a kinetic limitation at the electrode surface [39, 40].

The reference voltammogram measured in the absence of H_2AA was subtracted from the voltammograms in the presence of the analyte to obtain a better resolved ascorbic acid oxidation peak. A detection limit of 0.0160 mmol L^{-1} was determined according to IUPAC recommendations [41]. The SiO_2/MPTS/Au electrode showed an anodic potential and a detection limit for H_2AA determination that was similar to other researchers' work [40, 42–44].

Chronoamperometric study of ascorbic acid

The response time of the SiO_2/MPTS/Au electrode observed in Fig. 9 was about 1.0 s. This prompt response is followed by decay in the current density as observed after each ascorbic acid addition. This behavior is associated with the slow diffusion of ascorbic acid to the electrode surface before the electron transfer process [45]. In Fig. 9b inset, a linear response of the SiO_2/MPTS/Au electrode can be observed with a correlation coefficient of 0.9982 for n=45 in the concentration range between 0.0050 and 0.423 mmol L^{-1}. The detection limit determined was 2.842 μmol L^{-1} [41]. These values were comparable to results from other chronoamperometric sensors for H_2AA [46–48].

Determination of ascorbic acid in the presence of DA and UA

For the conventional electrodes (Fig. 10a), the oxidation responses for the three analytes cannot be defined clearly; however, they are observed at higher potential than for SiO_2/MPTS and SiO_2/MPTS/Au electrodes. The three anodic peaks at 0.184, 0.494, and 0.626 V are well defined and symmetrical, which can be attributed to the oxidation processes of H_2AA, DA, and UA, respectively (Fig. 10b). A peak around

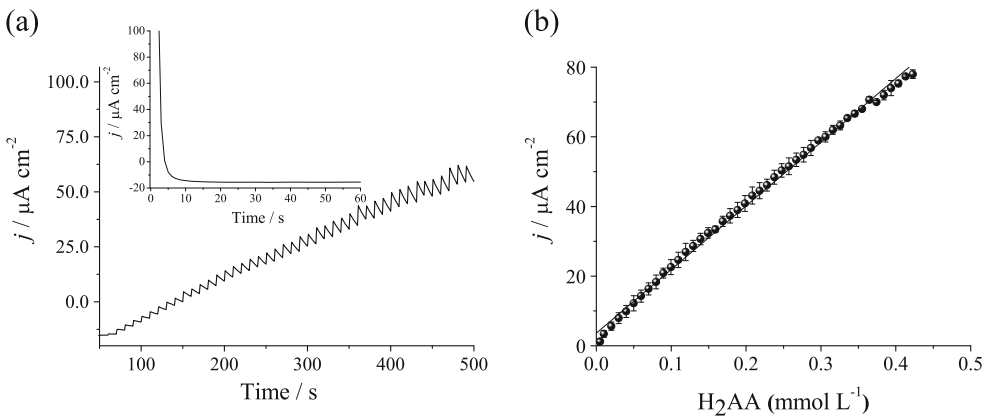

Fig. 9 **a** Chronoamperometric curves obtained for the SiO_2/MPTS/Au electrode after successive additions of 20 μL of 0.025 mol L^{-1} H_2AA in 50 mL of 0.10 mol L^{-1} phosphate buffer solution (pH 2.0). Applied potential= 0.180 V. *Inset*, chronoamperometric curve without H_2AA. **b** Plot of anodic current density (*j*) versus ascorbic acid concentration [H_2AA]

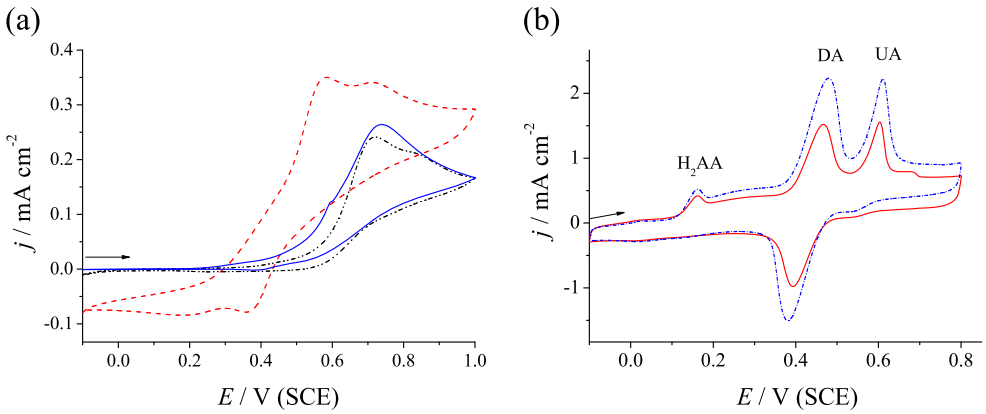

Fig. 10 **a** Cyclic voltammograms for platinum (*dashed line*), glass carbon (*solid line*), gold electrodes (*dash-dotted line*) and **b** for SiO_2/MPTS (*solid line*) and SiO_2/MPTS/Au (*dashed line*) electrodes in 0.10 mol L^{-1} phosphate buffer solution (pH 2.0) containing 2.0 mmol L^{-1} H_2AA, 1.0 mmol L^{-1} DA, and 1.0 mmol L^{-1} UA. A scan rate of 10 mV s^{-1} was used

0.380 V in the cathodic scan was attributed to the reduction of the byproduct resulting from the DA oxidation. The peaks of interest are well separated using the SiO_2/MPTS and SiO_2/MPTS/Au electrodes. The separation of the anodic peaks obtained for H_2AA/DA and H_2AA/UA are presented in Table 1 and compared with the data for other modified electrodes. The separation of peak potentials for H_2AA, DA, and UA could be attributed to their different adsorption affinities at the electrode surface; the SiO_2/MPTS/Au electrode yielded higher redox currents for the analytes probably due to the high surface area of the nAu.

Comparing Figs. 6b and 10b, one can notice a significant decrease in the oxidation current of H_2AA in the presence of DA and UA. A possible explanation can be related to a stronger interaction between nAu and dopamine/uric acid due to the NH_2 and NH groups in these compounds, respectively, leading to a higher affinity of these species at the electrode surface than for the ascorbic acid.

The determination of H_2AA, DA, and UA in solution was performed by changing the concentration of one compound while the other two concentrations were kept constant. This study was performed using the square wave voltammetry technique to obtain higher current sensitivity and better resolution. The results are shown in Fig. 11.

As can be seen in Fig. 11a, the H_2AA current peak increases proportionally with the H_2AA concentration when the concentrations of DA and UA were kept constant. No clear change in the DA and UA oxidation currents was observed while varying the H_2AA concentration. Similarly, the oxidation peak current of DA and UA increased proportionally with the increase in the DA or UA concentration, keeping the concentration of the other two compounds constant (as shown in Fig. 11b, c). Interestingly, the oxidation processes of H_2AA, DA, and UA at the SiO_2/MPTS/Au electrode could be observed simultaneously, and no peak overlapping was observed. The analytical parameters for the

Table 1 Comparison of ΔE_{pa}(DA-H_2AA) and ΔE_{pa}(UA-H_2AA) obtained by cyclic voltammetry for different modified electrodes

Electrode	Scan rate/mV s^{-1}	pH	ΔE_{pa} (mV) vs. SCE		Ref.
			DA-H_2AA	UA-AA	
GCE/poly-PVA	50	7.0[a]	140	280	
GCE/poly-ACBK	100	4.0[a]	200	368	[49]
GCE/poly-Evans Blue	100	4.5[a]	182	362	[50]
GCE/poly-NBAR	100	4.0[a]	195	364	[51]
Oxidized GCE	100	7.0[a]	163	290	[52]
GCE/ PtAu hybrid film	100	4.0[b]	120	290	[53]
Ceramic carbon	20	5.0[a]	200	350	[54]
GCE/poly-EBT	100	4,0[a]	210	380	[55]
β-CD-MWCNTs/Plu-nAu/GCE	50	7.0	132	131	[56]
Au-CNT/PGE	20	7.0	208	128	[57]
nAu/SAMs	20	5.0	110	–	[58]
SiO_2/MPTS/Au	10	2.0[a]	310	442	

[a]Phosphate buffer

[b]Glycine and $LiClO_4$ buffer

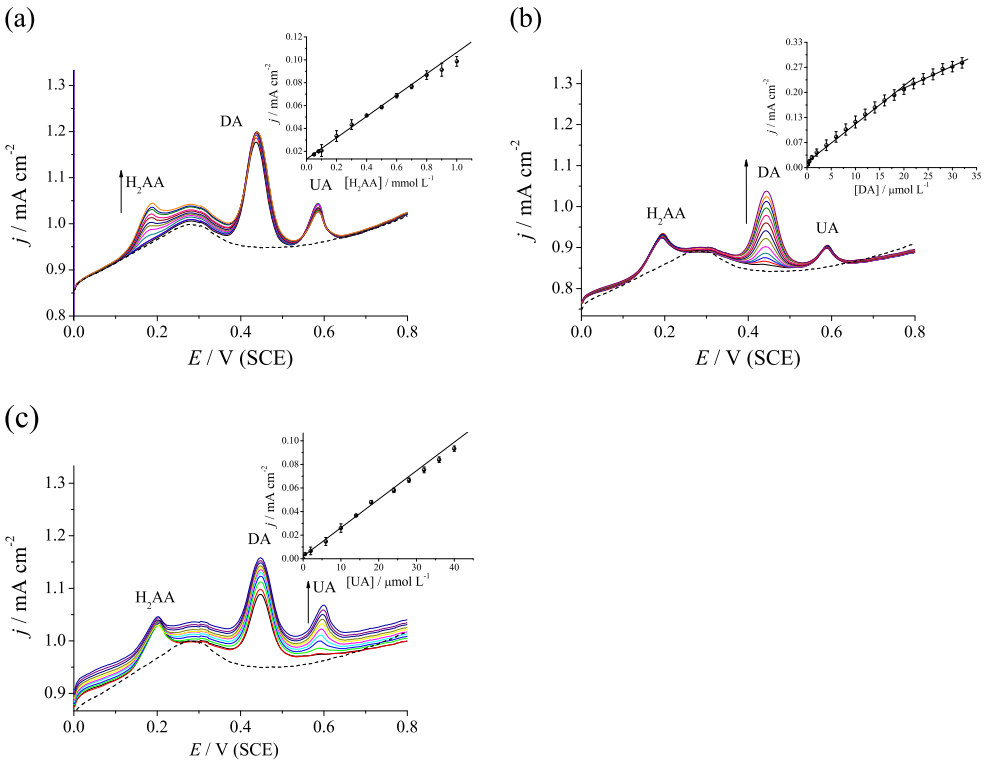

Fig. 11 Square wave voltammograms of **a** H_2AA concentrations: 0.050–1.0 mmol L^{-1}, with SiO_2/MPTS/Au electrodes in the presence of 20.0 μmol L^{-1} DA and 20.0 μmol L^{-1} UA. **b** DA concentrations: 0.20–20.0 μmol L^{-1}, with SiO_2/MPTS/Au electrodes in the presence of 2.0 mmol L^{-1} H_2AA and 20.0 μmol L^{-1} UA. **c** UA concentrations: 0.50–40.0 μmol L^{-1}, with SiO_2/MPTS/Au electrodes in the presence of 2.0 mmol L^{-1} H_2AA and 20.0 μmol L^{-1} DA. Supporting electrolyte: 0.10 mol L^{-1} phosphate buffer solution (pH 2.0). Square wave voltammogram in the absence of the analytes (*dash line*)

simultaneous determination of H_2AA, DA, and UA for the electrode prepared are listed and compared with the values for different modified electrodes in Table 2.

The detection limits were compared with results obtained by other researchers, and this comparison indicates that the SiO_2/MPTS/Au electrode can be used for simultaneous determination of H_2AA, DA, and UA [42–44].

Conclusions

SiO_2/MPTS with immobilized nAu was obtained by a simple preparation procedure using sol–gel chemistry. The gold nanoparticles in a functionalized silica network change the electrochemical behavior of the SiO_2/MPTS/Au electrode, favoring the electron transfer process of the studied species.

Table 2 Comparison between determination range and detection limit of different modified electrodes for the simultaneous determination of H_2AA, DA, and UA

Electrode	Determination range (μmol L^{-1})			Detection limit (μmol L^{-1})			Ref.
	H_2AA	DA	AU	H_2AA	DA	AU	
MWCNT–PEDOT film modified GCE	100–2,000	10–330	10–250	100	10	10	[59]
Chitosan-graphene-modified GCE	50–1,200	1–24	2.0–45	50	1.0	2.0	[60]
Tiron polymer film modified on GCE	4.0–792.0	0.2–45.8	0.06–166.0	1.79	0.07	0.021	[61]
Poly-nicotinic acid/GCE	75–3,000	0.37–16	0.741–230	15	0.09	0.18	[62]
Poly(acid chrome blue K)-modified GCE	50.0–1,000.0	1.0–200.0	1.0–120.0	10.0	0.5	0.5	[49]
Ordered mesoporous carbon/Nafion composite film-coated GCE	40–800	1.0–90	5–80	0.5	20	4.0	[63]
Poly-Evans Blue film-modified GCE	5.0–105	1.0–10	30–110	0.3	0.25	2.0	[50]
Gold nanoparticles-poly(luminol) hybrid	–	1.0–56.0	20–200	–	0.19	0.68	[56]
Gold nanoparticle-carbon nanotube-pyrolytic graphite	–	0.1–150	–	–	50	–	[57]
Self-assembled gold nanoparticle film	300–1,400	200–1,200	–	90.0	90.0		[58]
SiO_2/MPTS/Au	50.0–1,000.0	0.20–20.0	0.50–40.0	50.4	0.438	0.623	

These characteristics are desirable when this type of electrode is prepared for use in electrocatalytic and electroanalytical studies.

The SiO_2/MPTS/Au electrode was efficient in H_2AA determination as verified by cyclic voltammetry, chronoamperometry, and square wave voltammetry techniques. The voltammetric response to the oxidation process of H_2AA in the presence of DA and UA showed an adequate anodic peak separation for simultaneous detection of the analytes. The electrode prepared has shown promising characteristics to be used as an electrochemical sensor.

Acknowledgments The authors are indebted to Unifal-MG, CAPES, CNPq, and FAPEMIG for fellowships and financial support. We also thank the CME-UFRGS for use of the transmission electron microscopy facilities and Leliz T. Arenas for the TEM images.

References

1. Daniel MC, Astruc D (2004) Gold nanoparticles: assembly, supramolecular chemistry, quantum-size-related properties, and applications toward biology, catalysis, and nanotechnology. Chem Rev 104:293–346
2. Pastoriza-Santos I, Liz-Marzan LM (2009) *N, N*-Dimethylformamide as a reaction medium for metal nanoparticle synthesis. Adv Funct Mater 19:679–688
3. Kelly KL, Coronado E, Zhao LL, Schatz GC (2003) The optical properties of metal nanoparticles: the influence of size, shape, and dielectric environment. J Phys Chem B 107:668–677
4. Murray RW (2008) Nanoelectrochemistry: metal nanoparticles, nanoelectrodes, and nanopores. Chem Rev 108:2688–2720
5. Ghosh P, Han G, De M, Kim CK, Rotello VM (2008) Gold nanoparticles in delivery applications. Adv Drug Deliv Rev 60:1307–1315
6. Slowing II, Trewyn BG, Giri S, Lin VSY (2007) Mesoporous silica nanoparticles for drug delivery and biosensing applications. Adv Funct Mater 17:1225–1236
7. Huang XH, El-Sayed IH, Qian W, El-Sayed MA (2006) Cancer cell imaging and photothermal therapy in the near-infrared region by using gold nanorods. J Am Chem Soc 128:2115–2120
8. Castañeda MT, Alegret S, Merkoçi A (2007) Electrochemical sensing of DNA using gold nanoparticles. Electroanalysis 19:743–753
9. Pingarrón JM, Yáñez-Sedeño P, González-Cortés A (2008) Gold nanoparticle-based electrochemical biosensors. Electrochim Acta 53:5848–5866
10. Luo XL, Morrin A, Killard AJ, Smyth MR (2006) Application of nanoparticles in electrochemical sensors and biosensors. Electroanalysis 18:319–326
11. Hernandez-Santos D, Gonzalez-Garcia MB, Costa-Garcia A (2000) Electrochemical determination of gold nanoparticles in colloidal solutions. Electrochim Acta 46:607–615
12. White RJ, Luque R, Budarin VL, Clark JH, Macquarrie DJ (2009) Supported metal nanoparticles on porous materials. Methods and applications. Chem Soc Rev 38:481–494
13. Sun JM, Bao XH (2008) Textural manipulation of mesoporous materials for hosting of metallic nanocatalysts. Chemistry—a. Eur J 14:7478–7488
14. Collinson MM, Howells AR (2000) Sol–gels and electrochemistry: research at the intersection. Anal Chem 72:702a–709a
15. Walcarius A (2001) Electrochemical applications of silica-based organic–inorganic hybrid materials. Chem Mater 13:3351–3372
16. Walcarius A, Mandler D, Cox JA, Collinson M, Lev O (2005) Exciting new directions in the intersection of functionalized sol–gel materials with electrochemistry. J Mater Chem 15:3663–3689
17. Maroneze CM, Arenas LT, Luz RCS, Benvenutti EV, Landers R, Gushikem Y (2008) Meldola blue immobilized on a new SiO_2/TiO_2/graphite composite for electrocatalytic oxidation of NADH. Electrochim Acta 53:4167–4175
18. Pissetti FL, Francisco MSP, Landers R, Gushikem Y (2007) Phosphoric acid adsorbed on silica–ceria matrix obtained by sol–gel method: studies of local structure, texture and acid property. J Braz Chem Soc 18:976–983
19. Lucho AMS, Oliveira EC, Pastore HO, Gushikem Y (2004) 3-*n*-Propylpyridinium chloride silsesquioxane polymer film-coated aluminum phosphate and adsorption of cobalt(II)tetrasulphophthalocyanine: an electrocatalytic oxidation study of oxalic acid. J Electroanal Chem 573:55–60
20. Li Y, Lin X (2006) Simultaneous electroanalysis of dopamine, ascorbic acid and uric acid by poly (vinyl alcohol) covalently modified glassy carbon electrode. Sensors Actuators B Chem 115:134–139
21. Liu A, Wei M, Honma I, Zhou H (2006) Biosensing properties of titanate nanotube films: selective detection of dopamine in the presence of ascorbate and uric acid. Adv Funct Mater 16:371–376
22. Link S, El-Sayed MA (1999) Size and temperature dependence of the plasmon absorption of colloidal gold nanoparticles. J Phys Chem B 103:4212–4217
23. Sivanesan A, Kannan P, John SA (2007) Electrocatalytic oxidation of ascorbic acid using a single layer of gold nanoparticles immobilized on 1,6-hexanedithiol modified gold electrode. Electrochim Acta 52:8118–8124
24. Al-Oweini R, Ei-Rassy H (2009) Synthesis and characterization by FTIR spectroscopy of silica aerogels prepared using several Si $(OR)_4$ and $R''Si(OR')_3$ precursors. J Mol Struct 919:140–145
25. Liang XF, Xu YM, Sun GH, Wang L, Sun Y, Qin X (2009) Preparation, characterization of thiol-functionalized silica and application for sorption of Pb^{2+} and Cd^{2+}. Colloid Surf A-Physicochem Eng Asp 349:61–68
26. Feng X, Fryxell GE, Wang LQ, Kim AY, Liu J, Kemner KM (1997) Functionalized monolayers on ordered mesoporous supports. Science 276:923–926
27. Scully NM, O'Sullivan GP, Healy LO, Glennon JD, Dietrich B, Albert K (2007) Preparation of a mercaptopropyl bonded silica intermediate in supercritical carbon dioxide: synthesis, characterisation and chromatography of a quinine based chiral stationary phase. J Chromatogr A 1156:68–74
28. ElNahhal IM, Yang JJ, Chuang IS, Maciel GE (1996) Synthesis and solid-state NMR structural characterization of polysiloxane-immobilized thiol and thiol-amine ligands. J Non-Cryst Solids 208:105–118
29. Njoki PN, Lim IIS, Mott D, Park H-Y, Khan B, Mishra S, Sujakumar R, Luo J, Zhong C-J (2007) Size correlation of optical and spectroscopic properties for gold nanoparticles. J Phys Chem C 111:14664–14669
30. Wang J, Wang L, Di J, Tu Y (2009) Electrodeposition of gold nanoparticles on indium/tin oxide electrode for fabrication of a disposable hydrogen peroxide biosensor. Talanta 77:1454–1459
31. Wang JW, Wang LP, Di JW, Tu YF (2008) Disposable biosensor based on immobilization of glucose oxidase at gold nanoparticles electrodeposited on indium tin oxide electrode. Sensors Actuators B Chem 135:283–288
32. Jia JB, Wang BQ, Wu AG, Cheng GJ, Li Z, Dong SJ (2002) A method to construct a third-generation horseradish peroxidase biosensor: self-assembling gold nanoparticles to three-dimensional sol–gel network. Anal Chem 74:2217–2223

33. Raj CR, Ohsaka T (2003) Voltammetric detection of uric acid in the presence of ascorbic acid at a gold electrode modified with a self-assembled monolayer of heteroaromatic thiol. J Electroanal Chem 540:69–77
34. Hu G, Ma Y, Guo Y, Shao S (2008) Electrocatalytic oxidation and simultaneous determination of uric acid and ascorbic acid on the gold nanoparticles-modified glassy carbon electrode. Electrochim Acta 53:6610–6615
35. Chen ZF, Zu YB (2007) Simultaneous detection of ascorbic acid and uric acid using a fluorosurfactant-modified platinum electrode. J Electroanal Chem 603:281–286
36. Manzanares MI, Solis V, de Rossi RH (1997) Effect of cyclodextrins on the electrochemical behaviour of ascorbic acid on platinum electrodes in acidic and neutral solutions. J Electroanal Chem 430:163–168
37. dos Reis AP, Tarley CRT, Mello LD, Kubota LT (2008) Simple and sensitive electroanalytical method for the determination of ascorbic acid in urine samples using measurements in an aqueous cationic micellar medium. Anal Sci 24:1569–1574
38. Freire RS, Kubota LT (2002) Electrochemical behavior of the bis (2,2[prime or minute]-bipyridyl)copper(ii) complex immobilized on a self-assembled monolayer modified electrode for *l*-ascorbic acid detection. Analyst 127:1502–1506
39. Mazloum-Ardakani M, Habibollahi F, Zare HR, Naeimi H, Nejati M (2009) Electrocatalytic oxidation of ascorbic acid at a 2,2′-(1,8-octanediylbisnitriloethylidine)-bis-hydroquinone modified carbon paste electrode. J Appl Electrochem 39:1117–1124
40. Teixeira MFS, Ramos LA, Fatibello O, Cavalheiro ETG (2003) Carbon paste electrode modified with copper(II) phosphate immobilized in a polyester resin for voltammetric determination of L-ascorbic acid in pharmaceutical formulations. Anal Bioanal Chem 376:214–219
41. Committee AM (1987) Recommendations for the definition, estimation and use of the detection limit. Analyst 112:199–204
42. Rohani T, Taher MA (2009) A new method for electrocatalytic oxidation of ascorbic acid at the Cu(II) zeolite-modifled electrode. Talanta 78:743–747
43. Ojani R, Raoof JB, Norouzi B (2008) Cu(II) hexacyanoferrate (III) modified carbon paste electrode: application for electrocatalytic detection of nitrite. Electroanalysis 20:1996–2002
44. Wang JS, Wang JX, Wang Z, Wang SC (2006) Electrocatalytic oxidation of ascorbic acid at polypyrrole nanowire modified electrode. Synth Met 156:610–613
45. Lucho AMS, Pissetti FL, Gushikem Y (2004) Al_2O_3-coated 3-*N*-propylpyridinium chloride silsesquioxane polymer film: preparation and electrochemical property study of adsorbed cobalt tetrasulfophthalocyanine. J Colloid Interface Sci 275:251–256
46. Arenas LT, Gay DSF, Moro CC, Dias SLP, Azambuja DS, Costa TMH, Benvenutti EV, Gushikem Y (2008) Brilliant yellow dye immobilized on silica and silica/titania based hybrid xerogels containing bridged positively charged 1,4-diazoniabicyclo[2.2.2]octane: preparation, characterization and electrochemical properties study. Microporous Mesoporous Mater 112:273–283
47. Arvand M, Sohrabnezhad S, Mousavi MF, Shamsipur M, Zanjanchi MA (2003) Electrochemical study of methylene blue incorporated into mordenite type zeolite and its application for amperometric determination of ascorbic acid in real samples. Anal Chim Acta 491:193–201
48. Alfaya RVS, Gushikem Y, Alfaya AAS (2000) *N*-Propylpyridinium chloride silsesquioxane polymer film on graphite: electrochemical study of a hexacyanoferrate (II) ion immobilized electrode for oxidation of ascorbic acid. J Braz Chem Soc 11:281–285
49. Zhang R, Jin GD, Chen D, Hu XY (2009) Simultaneous electrochemical determination of dopamine, ascorbic acid and uric acid using poly(acid chrome blue K) modified glassy carbon electrode. Sensors Actuators B Chem 138:174–181
50. Lin LQ, Chen JH, Yao H, Chen YZ, Zheng YJ, Lin XH (2008) Simultaneous determination of dopamine, ascorbic acid and uric acid at poly (Evans Blue) modified glassy carbon electrode. Bioelectrochemistry 73:11–17
51. Lin XH, Zhang YF, Chen W, Wu P (2007) Electrocatalytic oxidation and determination of dopamine in the presence of ascorbic acid and uric acid at a poly (p-nitrobenzenazo resorcinol) modified glassy carbon electrode. Sensors Actuators B Chem 122:309–314
52. Thiagarajan S, Tsai TH, Chen SM (2009) Easy modification of glassy carbon electrode for simultaneous determination of ascorbic acid, dopamine and uric acid. Biosens Bioelectron 24:2712–2715
53. Thiagarajan S, Chen SM (2007) Preparation and characterization of PtAu hybrid film modified electrodes and their use in simultaneous determination of dopamine, ascorbic acid and uric acid. Talanta 74:212–222
54. Salimi A, Mamkhezri H, Hallaj R (2006) Simultaneous determination of ascorbic acid, uric acid and neurotransmitters with a carbon ceramic electrode prepared by sol–gel technique. Talanta 70:823–832
55. Yao H, Sun YY, Lin XH, Tang YH, Huang LY (2007) Electrochemical characterization of poly(eriochrome black T) modified glassy carbon electrode and its application to simultaneous determination of dopamine, ascorbic acid and uric acid. Electrochim Acta 52:6165–6171
56. Jia D, Dai JY, Yuan HY, Lei L, Xiao D (2011) Selective detection of dopamine in the presence of uric acid using a gold nanoparticles-poly (luminol) hybrid film and multi-walled carbon nanotubes with incorporated beta-cyclodextrin modified glassy carbon electrode. Talanta 85:2344–2351
57. Hu GZ, Chen L, Guo Y, Wang XL, Shao SJ (2010) Selective determination of L-dopa in the presence of uric acid and ascorbic acid at a gold nanoparticle self-assembled carbon nanotube-modified pyrolytic graphite electrode. Electrochim Acta 55:4711–4716
58. Raoof JB, Kiani A, Ojani R, Valiollahi R, Rashid-Nadimi S (2010) Simultaneous voltammetric determination of ascorbic acid and dopamine at the surface of electrodes modified with self-assembled gold nanoparticle films. J Solid State Electrochem 14:1171–1176
59. Lin K-C, Tsai T-H, Chen S-M (2010) Performing enzyme-free H_2O_2 biosensor and simultaneous determination for AA, DA, and UA by MWCNT–PEDOT film. Biosens Bioelectron 26:608–614
60. Han D, Han T, Shan C, Ivaska A, Niu L (2010) Simultaneous determination of ascorbic acid, dopamine and uric acid with chitosan-graphene modified electrode. Electroanalysis 22:2001–2008
61. Ensafi AA, Taei M, Khayamian T (2010) Simultaneous determination of ascorbic acid, dopamine, and uric acid by differential pulse voltammetry using tiron modified glassy carbon electrode. International Journal of Electrochemcal Science:116–130
62. Zhu X, Lin X (2009) Eletropolymerization of niacinamide for fabrication of electrochemical sensor: simultaneous determination of dopamine, uric acid and ascorbic acid. Chin J Chem:1103–1109
63. Zheng D, Ye J, Zhou L, Zhang Y, Yu C (2009) Simultaneous determination of dopamine, ascorbic acid and uric acid on ordered mesoporous carbon/Nafion composite film. J Electroanal Chem 625:82–87